

Article

Geopolymer Concrete Performance Study for High-Temperature Thermal Energy Storage (TES) Applications

Mohammad Rahjoo ^{1,*}, Guido Goracci ¹, Pavel Martauz ², Esther Rojas ³ and Jorge S. Dolado ^{1,4,*}

¹ Centro de Física de Materiales, CSIC-UPV/EHU, 20018 Donostia-San Sebastian, Spain; guido.goracci@ehu.eus

² Považská Cementáreň Cement Plant (PCLA), 01863 Ladce, Slovakia; martauz.p@pcl.sk

³ Plataforma Solar de Almería (PSA-CIEMAT), 28040 Madrid, Spain; esther.rojas@ciemat.es

⁴ Donostia International Physics Center (DIPC), 20018 Donostia-San Sebastian, Spain

* Correspondence: m.rahhoo@csic.es (M.R.); j.dolado@ehu.eus (J.S.D.); Tel.: +34-943-01-8772 (J.S.D.)

Abstract: Solar energy is an energy intermittent source that faces a substantial challenge for its power dispatchability. Hence, concentrating solar power (CSP) plants and solar process heat (SPH) applications employ thermal energy storage (TES) technologies as a link between power generation and optimal load distribution. Ordinary Portland cement (OPC)-based materials are widely used in sensible TES, but their use is limited to operation temperatures below 400 to 500 °C because of thermal degradation processes. This work proposes a geopolymer (GEO)-based concrete as a suitable alternative to OPC concrete for TES that withstands high running temperatures, higher than 500 °C. To this end, thermophysical properties of a geopolymer-based concrete sample were initially measured experimentally; later, energy storage capacity and thermal behavior of the GEO sample were modeled numerically. In fact, different thermal scenarios were modeled, revealing that GEO-based concrete can be a sound choice due to its thermal energy storage capacity, high thermal diffusivity and capability to work at high temperature regimes.



Citation: Rahjoo, M.; Goracci, G.; Martauz, P.; Rojas, E.; Dolado, J.S. Geopolymer Concrete Performance Study for High-Temperature Thermal Energy Storage (TES) Applications. *Sustainability* **2022**, *14*, 1937. <https://doi.org/10.3390/su14031937>

Academic Editor: Yongfeng Liu

Received: 24 December 2021

Accepted: 5 February 2022

Published: 8 February 2022

Publisher's Note: MDPI stays neutral with regard to jurisdictional claims in published maps and institutional affiliations.



Copyright: © 2022 by the authors. Licensee MDPI, Basel, Switzerland. This article is an open access article distributed under the terms and conditions of the Creative Commons Attribution (CC BY) license (<https://creativecommons.org/licenses/by/4.0/>).

Keywords: concentrated solar power; thermal energy storage; CSP; TES; OPC; geopolymer

1. Introduction

Solar energy has received more attention in recent years due to its dispatchability, abundance and scalability. Concentrated solar power (CSP) and solar process heat (SPH) are two ways of converting solar energy into power and heat.

The main challenge of using solar energy as the main source of energy is the intermittency of solar flux resulting in less thermal energy gain and so less heat or power generation. This impediment can be overcome by a mechanism called thermal energy storage (TES). The main roles of TES are to enhance plant foreseeability, control the demand and manage the state of generation as well as distribution.

Sensible heat storage and latent heat storage are the most commonly used techniques to store thermal energy. High-temperature applications mainly employ solid materials as they are more stable in the long term and, most importantly, cost-effective. In addition, problems such as freezing, evaporation or leakage will no longer be relevant.

The amount of stored thermal energy in a sensible TES is directly linked to specific heat capacity and temperature increase (ΔT), Equation (1). Therefore, the maximum extractable storage capacity is highly dependent on achievable ΔT and the constraints to reach the maximum temperature.

$$Q_s = m \times C_p \times \Delta T = \rho \times V \times C_p \times \Delta T, \quad (1)$$

- Stored sensible thermal energy Q_s (J).
- Mass of storage material (kg)
- Specific heat capacity C_p (J/kg °C).

- Temperature increase ΔT ($^{\circ}\text{C}$).
- Density ρ (kg/m^3).
- Volume of storage material V (m^3).

The relationship between the properties of storage material and the thermal conductivity can be expressed as:

$$k = \alpha \times \rho \times C_p \quad (2)$$

- Thermal conductivity k ($\text{W}/\text{m } ^{\circ}\text{C}$).
- Thermal diffusivity α unit (m^2/s).
- Volumetric heat capacity $C_{vol} = [\rho(T), C_p(T)]$ unit ($\text{J}/\text{m}^3 \text{ } ^{\circ}\text{C}$).

Thermal diffusivity and volumetric heat capacity are important factors in TES selection and design. In addition, the productivity of a TES system depends strongly on the thermal properties of the material used; the selected material needs to be efficient, capable and sustainable.

A promising material for sensible TES systems in CSP plants is concrete. Concrete is the resulting composite formed upon mixing cement binders, aggregates, admixtures and water. It is cheap and durable and requires low maintenance. Moreover, its ingredients are abundant and relatively well available all over the world. Ordinary Portland cement (OPC) is normally the cementitious binder used both in normal concrete and in TES devices based on concrete. Indeed, the applicability and performance of OPC concrete for TES have been largely investigated at research centers and validated in solar thermal applications [1–10]. Lating et al. [1,2] introduced and validated the thermal stability and storage performance of an improved OPC-based concrete (DLR) capable of operation between 200 and 400 $^{\circ}\text{C}$ for more than 370 thermal cycles. Likewise, Skinner et al. [6] studied and tested a lab-scale OPC-based developed concrete (UHPC) at temperatures between 400 and 500 $^{\circ}\text{C}$. Hoivik et al. [3] reported the most recent advance in employing concrete as TES. The team developed an improved OPC-based concrete (Heatcrete) as TES material capable of working at temperatures up to 380 $^{\circ}\text{C}$. Moreover, the performance and durability of Heatcrete after nearly two years of operations at the Masdar Institute Solar Platform (MISP) were confirmed.

However, CSP plants and solar process heat (SPH) applications can occasionally demand temperatures up to ~ 1000 $^{\circ}\text{C}$ [11], or at least temperatures much higher than those that OPC-based concretes can withstand. The durability and thermal properties of OPC-based composites are largely controlled by the most important hydration product of OPCs, the C-S-H gel (note that in Cement Chemist Notation C = CaO, S = SiO₂, H = H₂O). Unfortunately, C-S-H gel degrades at temperatures between ~ 400 and 600 $^{\circ}\text{C}$ [12,13], making the use of OPC-based TES modules highly risky at such temperatures.

In this scenario the question that arises is straightforward: can other cementitious binders be employed for this thermal energy storage application? Different cement families are known, among which belite cements (BCs) [14,15], calcium aluminate (CA) cements [16] and geopolymers (GEOs) [17–19] are just a few.

Nowadays GEO-based composites are receiving much attention due to environmental reasons (i.e., their CO₂ fingerprint is lower than that of OPCs). In essence, geopolymers contain a finely ground precursor that reacts with an alkali activator. Alkali activators include hydroxides, silicates, carbonates, sulfates, aluminates and oxides, that is to say, any soluble substances capable of providing alkali ions, increasing pH and promoting the dissolution of the precursor. When pure aluminosilicates and an alkali oxide/hydroxide are used, water does not take part in the reaction but may end up trapped in the resulting zeolite-like structure, the N-A-S-H (N = Na₂O, A = Al₂O₃). When certain CaO content is present in the reactants, apart from the N-A-S-H structure, the geopolymeric matrix can also include a calcium silicate hydrate gel rich in aluminum (C-A-S-H gel) with a certain resemblance to the C-S-H gel of ordinary Portland cement [20].

GEO concretes are in ready supply worldwide as they are mainly produced from secondary products and are also effective in reducing environmental impact [21]. There are

two main reasons why GEO-based concretes are appealing for energy storage applications. On the one hand, geopolymers-based concretes are capable of working at a higher temperature range and exhibit good thermal stability at elevated temperatures compared to OPC binders [22–25]. On the other hand, they provide a large content of nanoconfined water, something which is a hallmark for a stable and high heat capacity. In this sense, it should be noted that the molar contents for main products of OPC and geopolymers-based concretes are $C_{1.7}SH_{1.8}$ [26] and $N_{2.5}S_{3.5}A_2H_6$ [27], respectively, indicating a higher amount of water molecules for geopolymers (H_6) than for OPC ($H_{1.8}$).

This work aims to explore the potentiality of GEO concretes for working as TES modules at high temperatures. To this end, the specific heat and thermal diffusivity of GEO samples were measured experimentally in a large temperature range. Thereupon, a model of the TES module was developed using finite element analysis (FEA) by MATLAB [28]. To evaluate GEO concrete with other counterparts, two pioneer OPC-based concretes, DLR [2] and Heatcrete [3], were selected. For temperature ranges above 400 °C, the properties of counterparts [2,3] were extrapolated. By investigating different thermal scenarios and through comparing with considered OPC-based counterparts, the simulations demonstrate that GEO concretes have a more than acceptable thermal energy storage capacity along with an enhanced transient temperature distribution at high temperatures.

2. Materials and Methods

2.1. Sample Preparation

Industrially produced geopolymers hybrid cement containing 20% Portland cement clinker and 80% inorganic geopolymers from Považská Cementáreň was used as binder [29]. To prepare GEO concrete, $w/c = 0.6$ and 75%wt of steel slag aggregate were employed. Geopolymers help to maintain a stable and high heat capacity over different temperature ranges and slag maintains a proper thermal conductivity. Aggregates were crushed into fine powder (grain size < 0.25 mm). Therefore, powders were mixed using a mechanical blender at low speed (350 rpm) for 1 min to obtain a uniform dispersion of siliceous aggregates in the hybrid cement powder. Pure water was added and the solution was stirred at 750 rpm for 1 min and 30 s. Later, the solution was allowed to rest for 1 min and mixed again at 750 rpm for 1 min and 30 s. Mixes were cast in cylindrical silicone molds with $d = 4$ cm and sealed. After 24 h, the specimens were demolded and stored in an environmental chamber with 100% RH at room temperature for 28 days.

2.2. Specific Heat Capacity Measurement

Specific heat capacity of the sample was measured by differential scanning calorimetry (DSC) (Q2000TA Instrument). The experiment was carried out with a modulated method (MDSC); this technique provides information on both reversible and non-reversible thermal events. Consequently, MDSC allows signals coming from water evaporation (irreversible process) to be neglected and provides the real specific heat of the sample. Aluminum pans were used in the experiment and the sample weight was about 30 mg. Experiment was performed on heating between 100 and 400 °C with a heating rate of 3 °C/min and modulated with ± 0.48 °C every 60 s.

2.3. Thermal Diffusivity Measurement

The main part of this work is the comparison of the GEO sample with other cement-based materials. So, for the right evaluation of material efficiency, it is necessary to have a proper characterization of thermal diffusivity. However, depending on the material and the sample preparation, relevant deviations can be observed on the thermal diffusivity measured by different techniques [30,31].

Therefore, first, a reference pellet of hydrated OPC was measured by laser flash analysis (LFA), and the results were normalized to the literature values. Later, thermal diffusivity values of the GEO sample were multiplied by the normalization factor. Sample powders (size grain < 64 µm) were compressed by a manual hydraulic press (SPE-CAC)

applying 7 tons for 5 min. The pellet with a thickness of ~2 mm was investigated by LFA 457 Microflash. Measurements were made at room temperature, 50, 100, 200, 300, 400, 500, 600, 700, 800 and 900 °C. The heating rate was 10 °C/min. Five laser shots were performed for each temperature. Intervals between shots were 1.5 min to allow the homogenization of the temperature of the samples.

2.4. Geometry and Numerical Scheme

The geometry used for the numerical analysis was a square cubic block of concrete with an embedded tube. Block sizes were $100 \times 100 \times 100$ mm³ and the tube diameter was 25.4 mm. This layout with larger scale and more tubes is by far the best-known and most widely used scheme, Figure 1A.

The front face of the block was considered for numerical modeling and thermal analysis. However, to calculate the energy storage amount, which is a quantity dependent on mass and volume, outputs of the two-dimensional model were used and generalized to the module's volume and mass, Figure 1A.

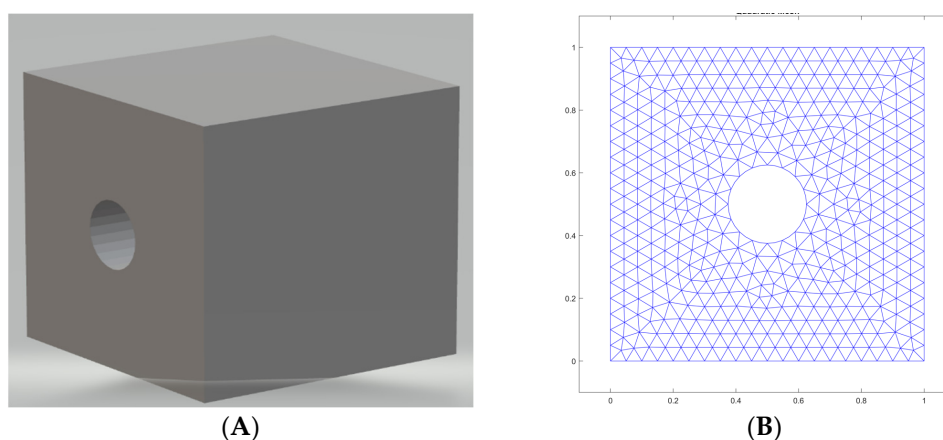


Figure 1. (A) Perspective view of geometry; module is $100 \times 100 \times 100$ mm³ volume with an embedded 25.4 mm (1") tube. (B) Quadratic triangular mesh used for finite element modeling (FEM) (scale 1:100, dimensions in mm).

To implement the problem in numerical form, the governing equations of the transient, conduction-dominant heat equation need to be derived. Simplifications were made regarding the model: no heat generation occurs inside the concrete block, heat does not vary over the length of the structure and radiation heat transfer is also neglected. Moreover, the tube's wall thickness is assumed to be so thin that its thermal resistance is negligible. The final form of the heat equation is as follows:

$$\frac{\partial}{\partial x} \left(k \frac{\partial T}{\partial x} \right) + \frac{\partial}{\partial y} \left(k \frac{\partial T}{\partial y} \right) = \rho c \frac{\partial T}{\partial t} \quad (3)$$

Additionally, the boundary and initial conditions are as follows:

- TES initially at a uniform temperature ($T(x, y, 0) = T_{initial}$);
- Specified temperature—tube side T_{inlet} ($T(r = r_{out}, t) = T_{inlet}$);
- Specified heat flux—insulated boundary ($k \frac{\partial T(x = 0, L, t)}{\partial x} = 0$ and $k \frac{\partial T(y = 0, L, t)}{\partial y} = 0$).

2.5. Methodology

In this study, the following steps were performed during numerical analysis:

1. For the selected OPC concrete counterparts, DLR [2] and Heatcrete [3], there was no information for their thermal properties at $T > 400$ °C in state of the art. For the sake of comparing the results of GEO with other samples at 400 °C $< T \leq 700$ °C, two fictitious OPCs (OPC-1 and OPC-2) were introduced. The thermal properties of

OPC-1 and OPC-2 correspond to the extrapolated thermal properties of Heatcrete and DLR, respectively. Further information is provided in Appendices A and B.

2. Quadratic triangular mesh was adopted for the numerical scheme (Figure 1B). Accordingly, the temperature for all nodes linked to each element can be calculated at any timestep. The term “ $T_{average}$ ” was introduced as the average temperature of all elements in the mesh region. $T_{average}$ strongly depends on the initial and boundary conditions plus transient behavior of materials. This parameter is an essential factor for the evaluation of charging/discharging time and the estimation of the amount of stored energy and transient heat distribution in the TES module. Grid test analysis was applied to the mesh to guarantee consistency of the results. See Appendix C.
3. “ T_{inlet} ” was defined as tube wall temperature inside the block. It was used to evaluate the TES module in different scenarios of charging and discharging.
4. Since the performance of a TES device is deeply reliant on its characteristics under transient operation, Figure 2 shows calculated transient temperatures, T_{1-4} , at different intervals from the tube wall. See Appendix C.

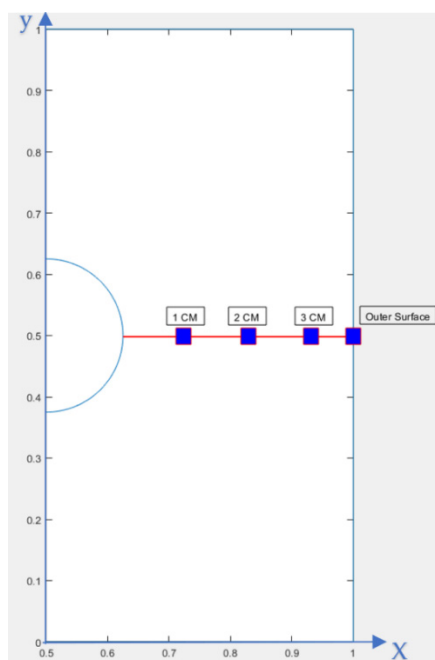


Figure 2. Points marked on the XY plane to monitor the temperature changes at specified distances from the tube wall, T_1 , T_2 , T_3 and T_4 . (scale 1:100 mm).

3. Results

3.1. Experimental Results

The MDSC-measured values of specific heat capacity for GEO represent a consistent behavior versus temperature rise. Data for other samples, DLR [2] and Heatcrete [3] show an increasing trend with temperature rise (Figure 3). Measured α values for GEO show a more stable trend versus temperature compared to OPC-1 and OPC-2 (Figure 4). The thermal diffusivity (α) describes the rate of temperature spread through a material and is for characterizing unsteady heat conduction behavior. In fact, for temperatures more than 400 °C, the GEO concrete is expected to have higher thermal diffusivity than OPC-1 and OPC-2. Values for thermal conductivity, specific heat capacity and density of samples are tabulated in Appendix A. For temperatures $T > 400$ °C, extrapolated values of DLR [2] and Heatcrete [3] concretes are used. Moreover, graphs of density (kg/m³), specific heat (J/kg °C), thermal conductivity (W/m °C), thermal diffusivity (m²/s) and volumetric heat capacity (J/m³ °C) as a function of temperature in the range of 100 to 700 °C are presented in Appendix B; the graphs are based on values presented in Appendix A and Equation (2).

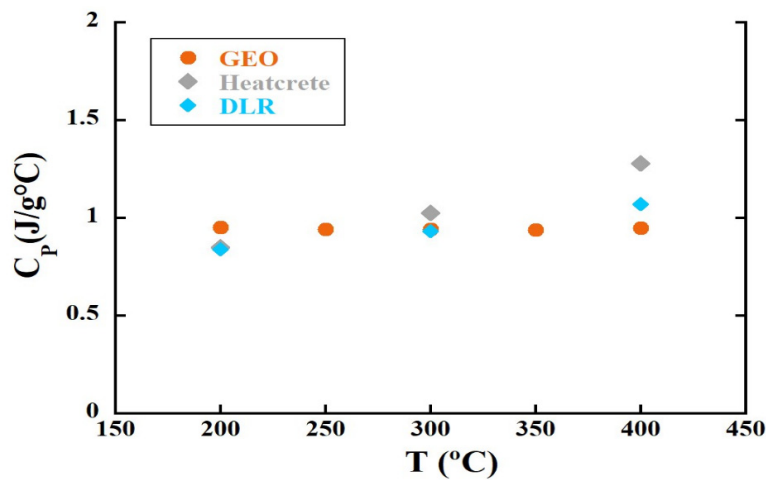


Figure 3. Measured specific heat of the GEO concrete, compared to other leading samples DLR [2] and Heatcrete [3].

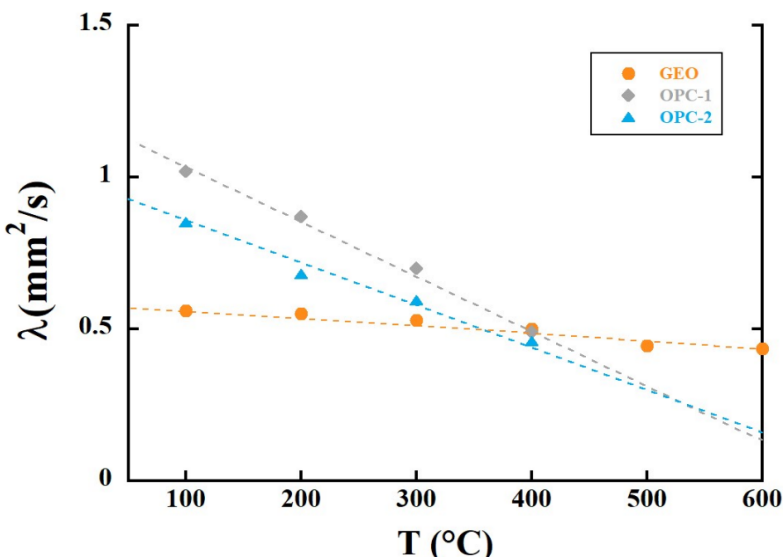


Figure 4. Measured thermal diffusivity of the GEO concrete, compared to defined samples OPC-1 and OPC-2. The dashed lines are guides to the eye to notice the trends.

3.2. Numerical Results—Average Temperature

In the beginning, a low temperature regime with $T_{inlet} = 400\text{ }^{\circ}\text{C}$ and $T_{initial} = 250, 300$ and $350\text{ }^{\circ}\text{C}$ was considered. Then, $T_{average}$ for different modules was calculated after 6 h of heating. In low temperature range, OPC-1 reaches the highest $T_{average}$ after 6 h. However, as the $T_{initial}$ increases, the difference between $T_{average}$ values of TES modules becomes smaller (Table 1).

Afterward, a high temperature regime was considered. $T_{average}$ was calculated for GEO, OPC-1 and OPC-2 for $T_{inlet} = 700\text{ }^{\circ}\text{C}$ and $T_{initial} = 250\text{--}650\text{ }^{\circ}\text{C}$ with $50\text{ }^{\circ}\text{C}$ intervals. In this scenario, the GEO module outperforms for $T_{initial} > 350\text{ }^{\circ}\text{C}$ because of having higher thermal diffusivity at higher temperatures. Concisely, the calculated average temperature of GEO greatly depends on the inlet and initial temperatures of TES modules. Results are shown in Table 2.

Table 1. Average temperature reached after 6 h for $T_{inlet} = 400\text{ }^{\circ}\text{C}$.

| $T_{inlet} = 400\text{ }^{\circ}\text{C}$, after 6 h | $T_{initial} = 250\text{ }^{\circ}\text{C}$ | $T_{initial} = 300\text{ }^{\circ}\text{C}$ | $T_{initial} = 350\text{ }^{\circ}\text{C}$ |
|---|---|---|---|
| OPC-1 | 277.3 | 316.9 | 357.8 |
| OPC-2 | 270.3 | 313.1 | 356.4 |
| GEO | 268.4 | 312.3 | 356.1 |

Table 2. Average temperature reached after 6 h for $T_{inlet} = 700\text{ }^{\circ}\text{C}$.

| $T_{inlet} = 700\text{ }^{\circ}\text{C}$ after 6 h | Initial Temperatures $^{\circ}\text{C}$ | | | | | | | | |
|--|---|-------|-------|-----|-------|-------|-------|-------|-------|
| | 250 | 300 | 350 | 400 | 450 | 500 | 550 | 600 | 650 |
| OPC-1 | 317.9 | 356.1 | 395.7 | 437 | 479.7 | 522.9 | 566.6 | 610.7 | 655.2 |
| OPC-2 | 305.9 | 348.1 | 390.8 | 434 | 477.5 | 521.4 | 565.6 | 610.2 | 655.0 |
| GEO | 305.1 | 349.0 | 392.9 | 436 | 480.6 | 524.5 | 568.4 | 612.3 | 656.1 |

3.3. Numerical Results—Energy Storage

Stored thermal energy E (kJ) after 6 h of heating up the TES modules was calculated for both low and high T_{inlet} conditions. Different initial temperatures were considered. As could be predicted from Tables 1 and 2, for $T_{inlet} = 400\text{ }^{\circ}\text{C}$, the GEO module shows E values close to those of the OPC-2 module, even though the values of E are ~24% smaller than those of OPC-1 (Figure 5A). Regarding the high temperature range ($T_{inlet}=700\text{ }^{\circ}\text{C}$), an improvement in GEO results is observed; however, the amount of energy stored for GEO is still less than that for the OPC-1 sample (Figure 5B). As mentioned previously, the properties for OPC-1 and OPC-2 are extrapolated from concretes, and there is no evidence that these specimens can operate in this temperature range.

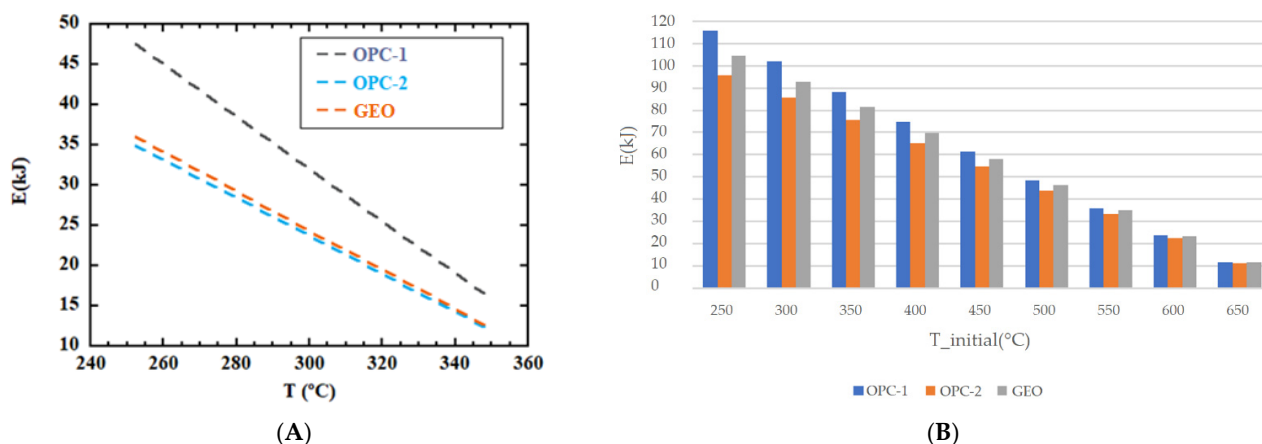


Figure 5. (A) Energy stored (kJ) for $T_{inlet} = 400\text{ }^{\circ}\text{C}$, charging for 6 h and different initial temperatures. (B) Energy stored (kJ) for $T_{inlet} = 700\text{ }^{\circ}\text{C}$, charging for 6 h and different initial temperatures.

4. Discussion

In the previous section, several thermal properties of the GEO samples were disclosed as a function of temperature, confirming the expected good behavior of GEO concretes at high temperatures. Now, the numerical experiments will go a step further and will evaluate the performance of the modules under charging and discharging cycles.

To simulate the charge and discharge scenarios, T_{inlet} was considered as a stepwise approach of distinct stages. In this way, $T_{inlet} = T_{max}$ for the charging process and $T_{inlet} = T_{min}$ for the discharge process. T_{max} and T_{min} are operating temperature scenarios.

Each complete charge/discharge cycle takes 12 h. Modeling was conducted with temperature data of two solar power plants currently operating. The first is the 1.0 MWh Nest storage pilot at the Masdar Institute Solar Platform (MISP) in Abu Dhabi, United Arab Emirates [3], operating between 290 and 390 $^{\circ}\text{C}$ with thermo-oil as heat transfer

fluid. The second is the Solar Two power tower pilot in California, USA [32], along with GEMASOLAR in Seville, Spain [33], with molten salt as heat transfer fluid. $T_{initial} = 290\text{ }^{\circ}\text{C}$ and $T_{inlet} = 565\text{ }^{\circ}\text{C}$ were studied.

Afterward, a high temperature regime ($T = 290\text{--}700\text{ }^{\circ}\text{C}$) was considered to evaluate the GEO module's behavior at high temperature ranges. The TES industry is always developing, and new applications are always offered depending on the capability of materials; hence, for the upcoming TES technologies, it is suitable to anticipate the thermal behavior of the material.

4.1. Case 1 (Operating Temperature $T = 290\text{--}565\text{ }^{\circ}\text{C}$)

In Figure 6A, the calculated $T_{average}$ of the TES modules is shown. An attempt has been made to estimate the time required for initial setup and reaching the inlet temperature, $T_{inlet} = 565\text{ }^{\circ}\text{C}$. After about 280 h, $T_{average}$ was compared for different modules (Figure 6B). OPC-1 module obtained the highest average temperature, followed by GEO and then OPC-2.

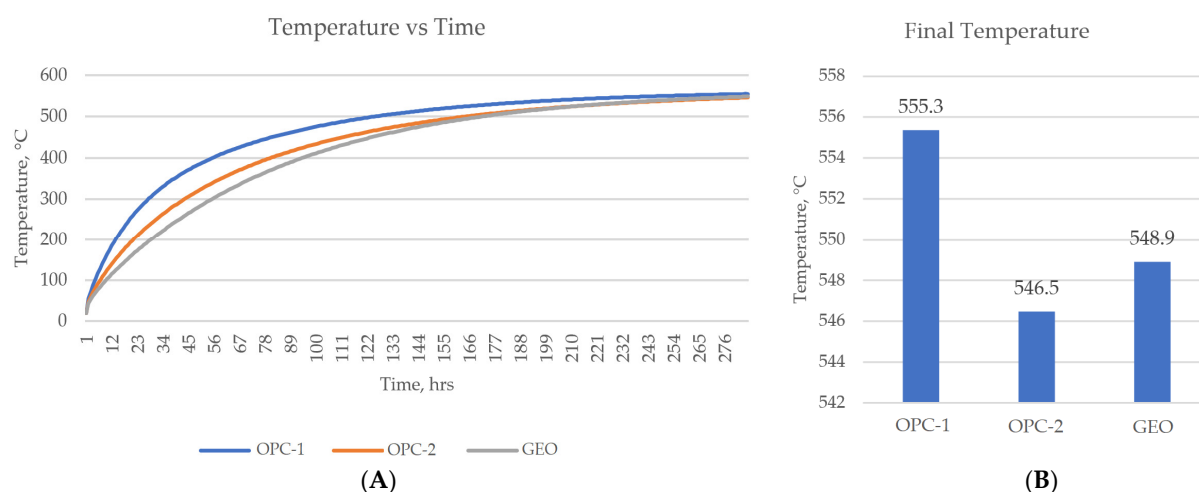


Figure 6. (A) Commissioning for $T_{inlet} = 565\text{ }^{\circ}\text{C}$, charging for 280 h. (B) Temperature at final time.

Figure 7A shows the charging and discharging cycles for three TES modules. After ~50 cycles, modules work at a defined temperature range. Observation shows that the GEO module works in a higher temperature margin, but as shown in Figure 7B, the OPC-1 module works with improved ΔT values for both charging and discharging at a specified time.

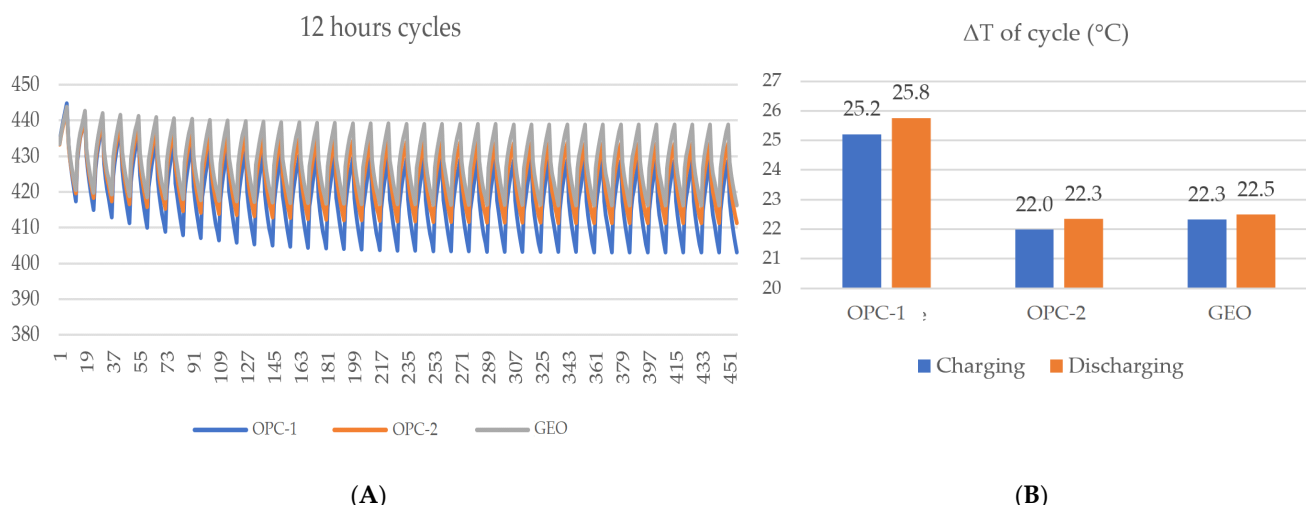


Figure 7. (A) Charging/discharging cycles for $T_{inlet} = 565/290\text{ }^{\circ}\text{C}$, $T_{initial} = 427.5\text{ }^{\circ}\text{C}$. (B) Temperature difference of each charging/discharging after stabilizing period, cycle > 50.

Temperatures inside the TES body at specified intervals along the X-axis between the tube's surface and right edge, as mentioned in Figure 2, were estimated. After the $T_{initial} = 290^{\circ}\text{C}$ and $T_{inlet} = 565^{\circ}\text{C}$ were determined and the charging process was performed for 6 h, OPC-1 achieved the highest temperature in all intervals, $T_{1,2,3}$ and 4. At 1 cm from the surface of the tube and after 3.5 h, the GEO sample has a higher temperature than OPC-2 (Figure 8). This is because the temperature at that point is reaching the value where the thermal diffusivity of the GEO sample is higher.

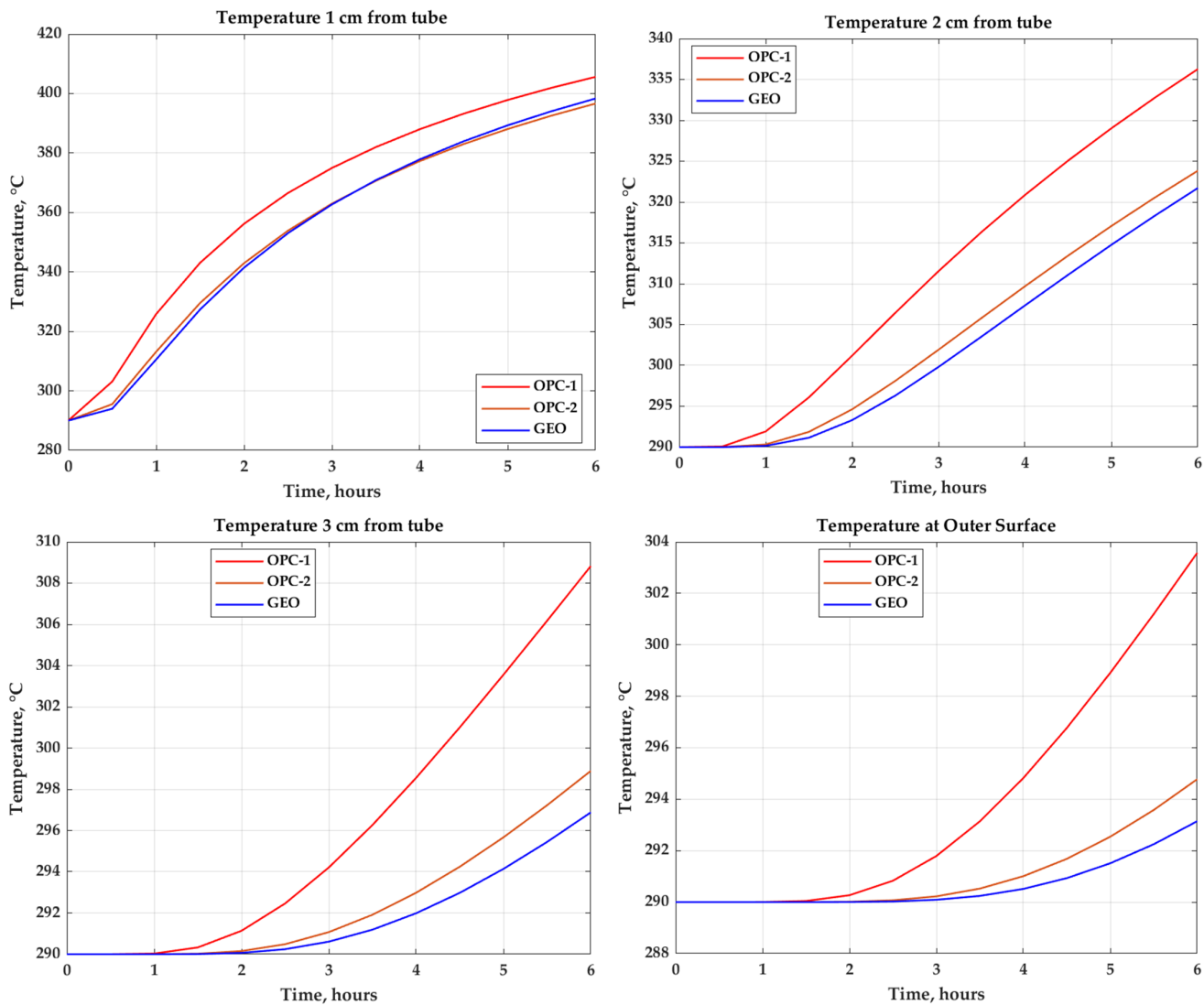


Figure 8. Transient temperature at different intervals after 6 h for $T_{inlet} = 565^{\circ}\text{C}$ and $T_{initial} = 290^{\circ}\text{C}$.

The temperature distribution map, heat flux vector field and calculated average temperature for 6 h of charging and discharging are shown in Figures 9 and 10. In the charging scenario, the OPC-1 sample has the highest average temperature, and OPC-2 and GEO samples have relatively close average temperatures, with less than 1 °C difference. For the discharge scenario of Figure 10, the calculated $T_{average}$ of GEO is more improved than that of OPC-2 even though the values for OPC-1 are more suitable. It is worth mentioning that these calculations have been completed knowing there is no information for properties of counterparts [2,3] above 400 °C and assuming the functionality of OPC-1 and OPC-2 at high temperatures. In fact, OPC-based concretes degrade at temperatures above 400–450 °C [12,13]. This makes GEO concrete a potentially good choice that is able to operate in a wider temperature range, greater ΔT , and consequently greater energy storage capacity.

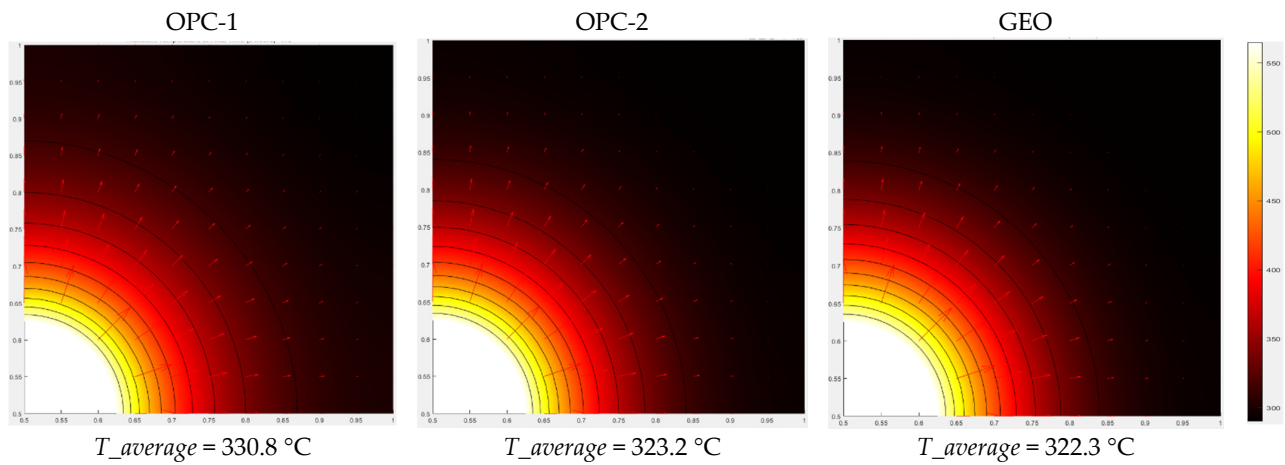


Figure 9. Transient temperature, heat flux distribution and average temperature after 6 h for $T_{inlet} = 565\text{ }^{\circ}\text{C}$ and $T_{initial} = 290\text{ }^{\circ}\text{C}$.

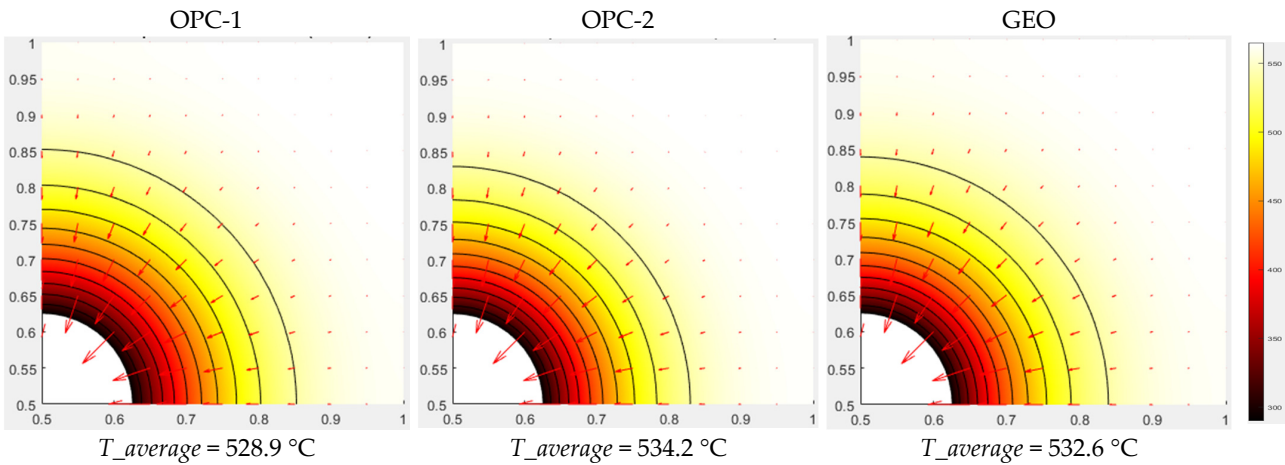


Figure 10. Transient temperature, heat flux distribution and average temperature after 6 h for $T_{inlet} = 290\text{ }^{\circ}\text{C}$ and $T_{initial} = 565\text{ }^{\circ}\text{C}$.

4.2. Case 2 (Operating Temperature $T = 290\text{--}700\text{ }^{\circ}\text{C}$)

Assuming that OPC-based samples are able to operate in this temperature range, the GEO concrete has an acceptable behavior. The GEO module reached the highest average temperature for $T_{inlet} = 700\text{ }^{\circ}\text{C}$ and after about 300 h (Figure 11A,B). Although Figure 12A,B shows the same trend analyzed in case 1, the temperature difference of charging/discharging after the stabilizing period, cycle > 50 , for GEO is about 3% lower than that for OPC-1 and 6% higher than that for OPC-2.

Figure 13 shows the temperature values at different intervals inside the TES block for $T_{inlet} = 700\text{ }^{\circ}\text{C}$ and $T_{initial} = 290\text{ }^{\circ}\text{C}$ and after 6 h. Unlike Case 1, this setup shows that GEO achieves a higher temperature than OPC-2 at 1 cm from the surface of the tube and a temperature close to that of OPC-2 at 2 cm. However, the values of OPC-1 are greater than those of OPC-2 and GEO. After another scenario was defined and the TES modules were heated for 96 h to estimate $T_{1,2,3,4}$ (Figure 14), GEO achieved the highest temperature in the 1 cm interval and a higher temperature than OPC-2 in the rest of the intervals. The final average temperatures for different TESs were 587.1, 568.7 and 587.3 $^{\circ}\text{C}$ for OPC-1, OPC-2 and GEO, respectively. The results confirm what has been raised about the heat capacity and thermal stability of geopolymers-based concrete at higher temperature ranges [24,25]. However, in this regime, an overestimation of the specific heat of OPC-1 and OPC-2 participants is highly expected (Appendix B, specific heat ($\text{J}/\text{kg }^{\circ}\text{C}$) as a function of temperature).

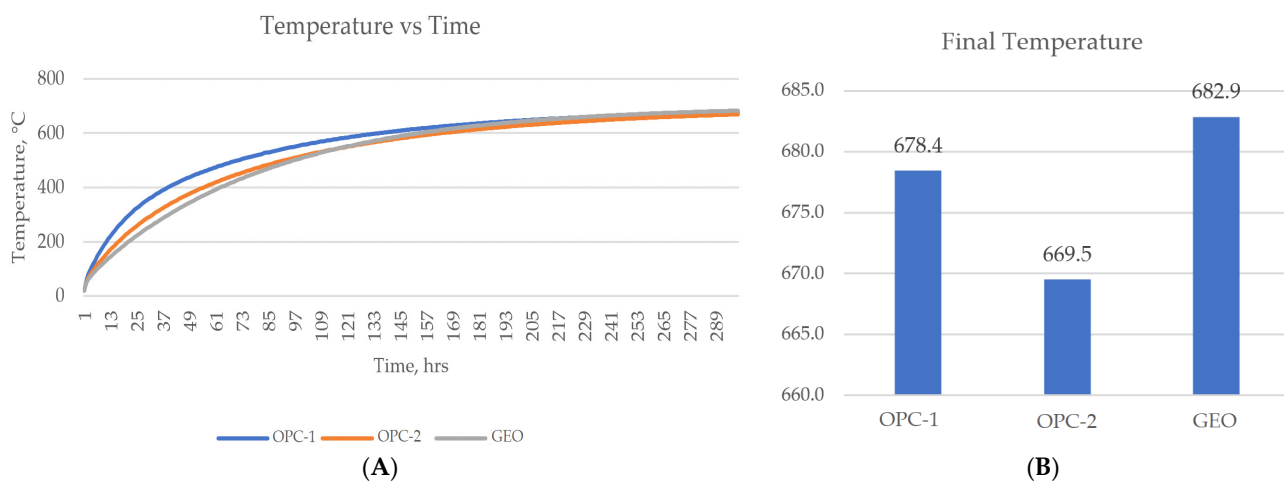


Figure 11. (A) Commissioning for $T_{inlet} = 700\text{ }^{\circ}\text{C}$, charging for 300 h. (B) Average temperature of TES modules at final time.

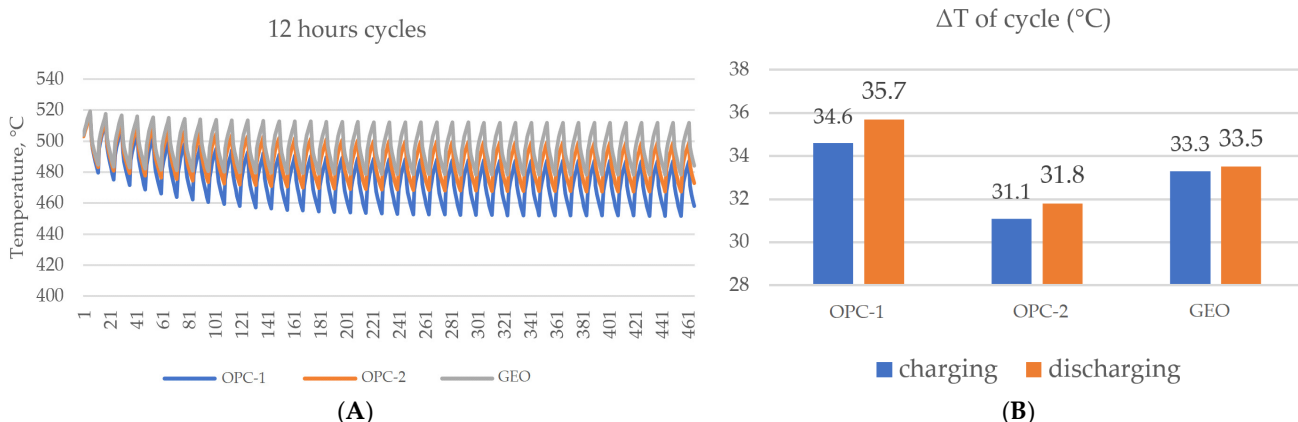


Figure 12. (A) Charging/discharging cycles for $T_{inlet} = 700/290\text{ }^{\circ}\text{C}$, $T_{initial} = 495\text{ }^{\circ}\text{C}$. (B) Temperature difference of charging/discharging after stabilizing period, cycle > 50.

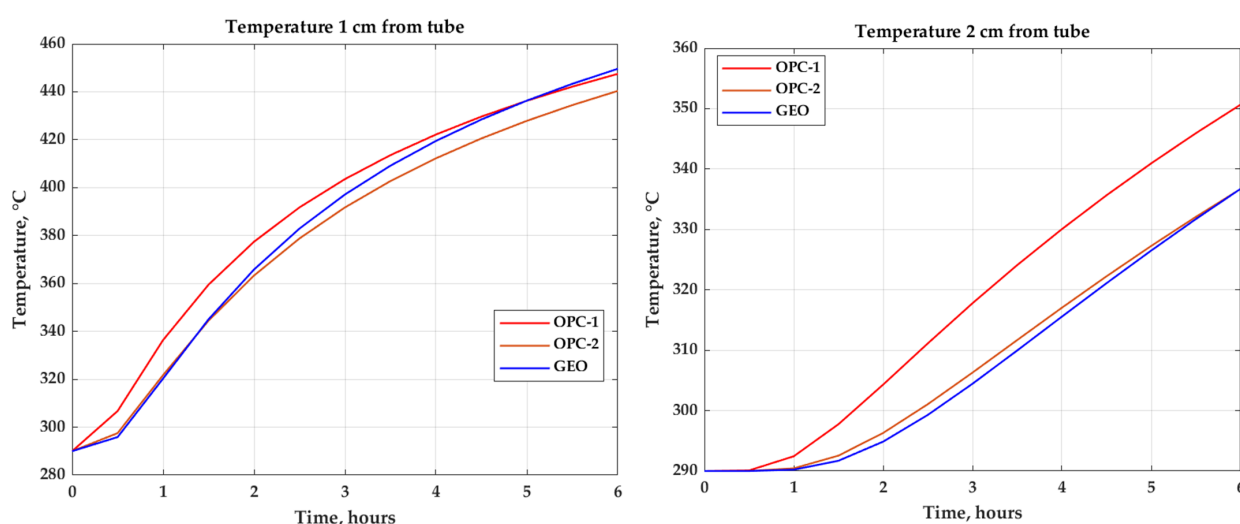


Figure 13. Cont.

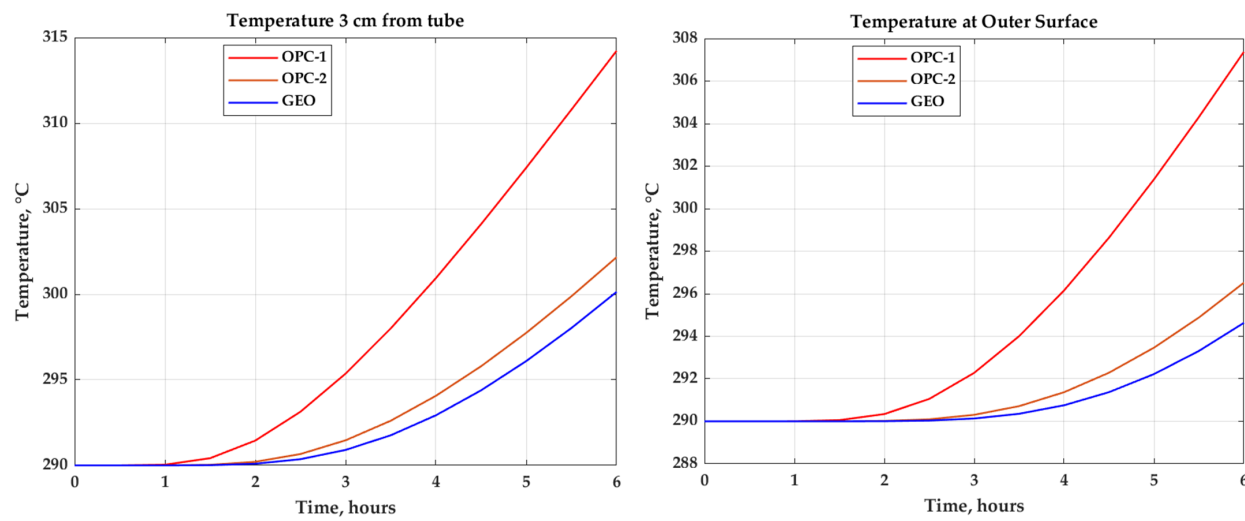


Figure 13. Transient temperature of different intervals along X-axis versus time after 6 h for $T_{inlet} = 700\text{ }^{\circ}\text{C}$ and $T_{initial} = 290\text{ }^{\circ}\text{C}$.

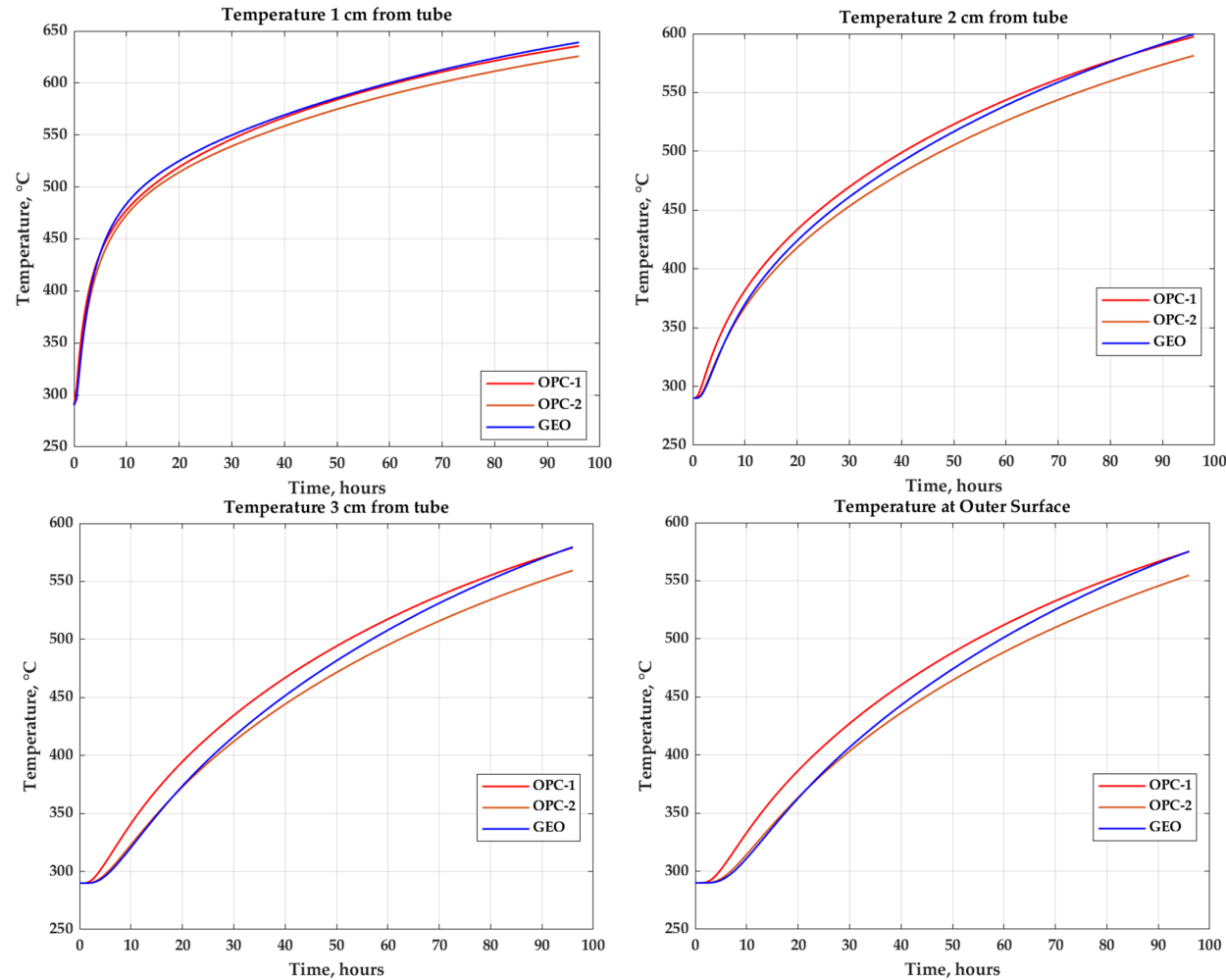


Figure 14. Transient temperature of different intervals along X-axis versus time after 96 h for $T_{inlet} = 700\text{ }^{\circ}\text{C}$ and $T_{initial} = 290\text{ }^{\circ}\text{C}$. Calculated average block temperatures are 587.1, 568.7 and 587.3 $^{\circ}\text{C}$ for OPC-1, OPC-2 and GEO.

Temperature distribution contours and heat flux vectors for charging and discharging setups (Figures 15 and 16) show the same trend as Case 1. The OPC-1 sample has the highest

average temperature, followed by the GEO sample and then the OPC-2 sample. However, in this scenario, the values of average temperature for GEO concrete are closer to those of OPC-1, showing about 1 °C difference with OPC-1 and 5 °C difference with OPC-2 (Figure 15).

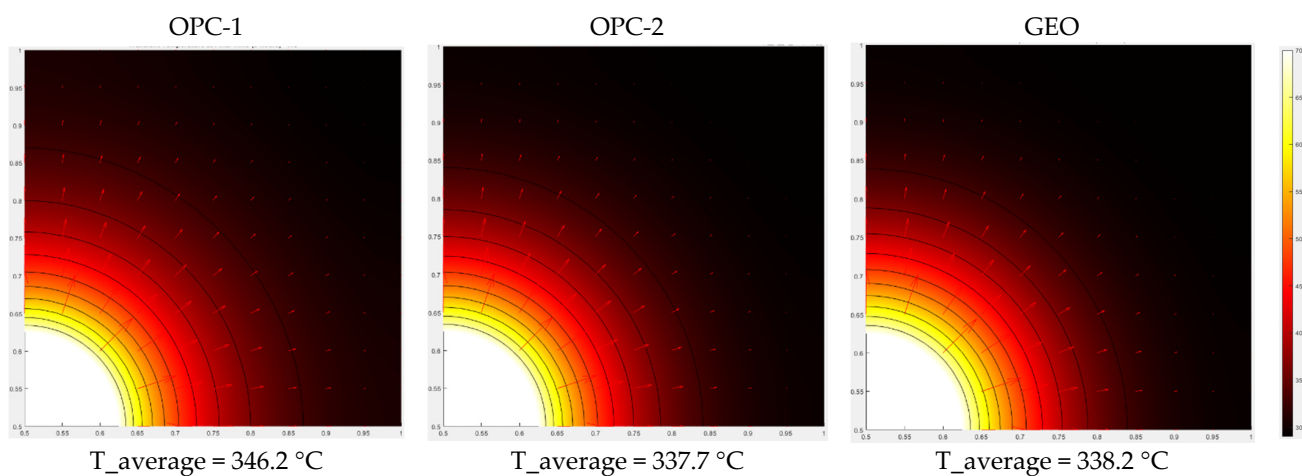


Figure 15. Transient temperature, heat flux distribution and average temperature after 6 h for $T_{inlet} = 700\text{ }^{\circ}\text{C}$ and $T_{initial} = 290\text{ }^{\circ}\text{C}$.

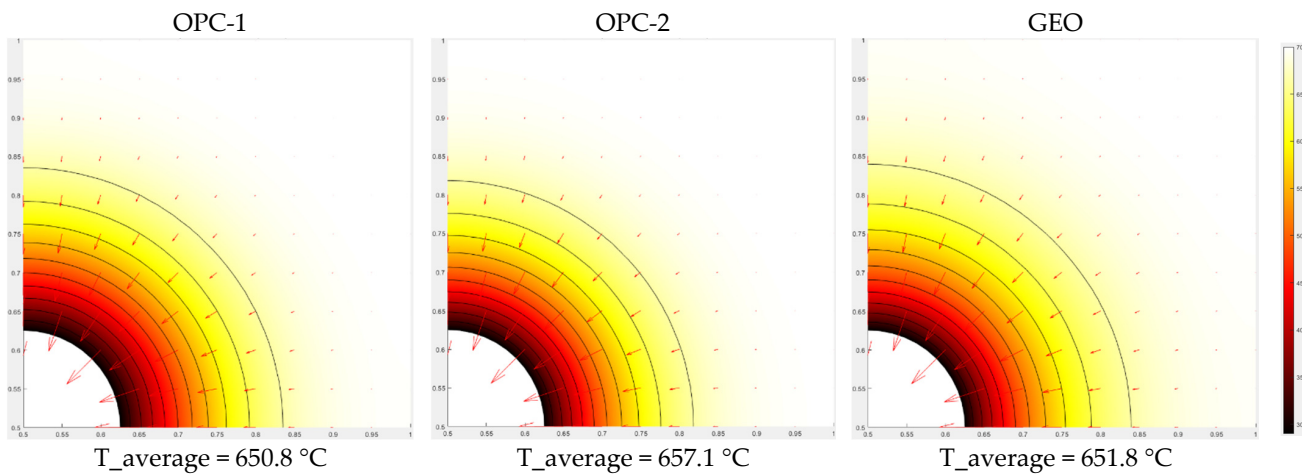


Figure 16. Transient temperature, heat flux distribution and average temperature after 6 h for $T_{inlet} = 290\text{ }^{\circ}\text{C}$ and $T_{initial} = 700\text{ }^{\circ}\text{C}$.

5. Conclusions

This work studies the possibility of substituting the OPC-based concrete with geopolymer-based concrete for thermal energy storage applications, specifically at high temperature ranges. GEO-based concretes have higher resistance to elevated temperatures, which brings the opportunity to operate in a wider temperature range and thus provides more thermal storage capacity. In particular, the experimental measurements show that specific heat of the GEO sample is nearly $1000\text{ W s/kg }^{\circ}\text{C}$ and is stable up to $600\text{ }^{\circ}\text{C}$, and its thermal diffusivity is $5 \times 10^{-7}\text{ m}^2/\text{s}$ and is greater than that of OPC counterparts at temperatures $T > 400\text{ }^{\circ}\text{C}$. Moreover, computational results reveal that the use of GEO-based concretes as a storage material can improve the storage capacity and transient temperature distribution of TESs, specifically at high temperatures. At high temperature regimes, the highest average temperature is obtained by GEO concrete, and the thermal energy storage capacity and temperature difference (ΔT) in cyclic charging and discharging operations are in a very acceptable range for TES material. Altogether, this work demonstrates that GEO concretes are a promising alternative so that CSP and SPH industries can work at higher temperatures with geopolymer-based materials. Of course, future steps should include the design of

prototypes to scale up the obtained values to real operating conditions. Paying attention to the further reduction in the use of cementitious materials and utilizing alkali activation of calcined clays or fly ashes in the development of thermal storage material also increase sustainability and should be considered in the future.

Author Contributions: Conceptualization, J.S.D. and E.R.; methodology, M.R. and G.G.; investigation, M.R., G.G., E.R., P.M. and J.S.D.; writing—original draft preparation, M.R.; writing—review and editing, M.R., G.G., E.R., P.M. and J.S.D.; supervision, J.S.D. and E.R.; funding acquisition, J.S.D. and E.R. All authors have read and agreed to the published version of the manuscript.

Funding: This work was born under the umbrella of the project “Energy storage solutions based on concrete (E-CRETE)” (RTI2018-098554-B-I00) funded by MCIN/AEI/10.13039/501100011033 (Program I+D+i RETOS INVESTIGACIÓN 2018). Mohammad Rahjoo acknowledges the grant PRE2019-087676 funded by MCIN/AEI/10.13039/501100011033 and co-financed by the European Social Fund under the 2019 call for grants for predoctoral contracts for the training of doctors contemplated in the State Training Subprogram of the State Program for the Promotion of Talent and its Employability in R&D&I, within the framework of the State Plan for Scientific and Technical Research and Innovation 2017–2020. Besides, the economic support from POVAZSKA is also acknowledged.

Institutional Review Board Statement: Not applicable.

Informed Consent Statement: Not applicable.

Data Availability Statement: Not applicable.

Acknowledgments: We acknowledge the computing resources and time made available by Donostia International Physics Center (DIPC) (Donostia, Spain).

Conflicts of Interest: The authors declare no conflict of interest.

Appendix A. Main Thermal Properties of Concrete Samples Used in This Study

The properties used in this work are given in the table below. These properties include thermal conductivity, specific heat capacity and density of the samples. Properties obtained for OPC-2 are the properties of DLR [2]; the same reference formulas have been used for temperatures above 400 °C. Properties of OPC-1 are curve-fitted, for $T \leq 400$ °C from Heatcrete [3], and extrapolated for $T > 400$ °C. R-squared (R^2) values are considered to be higher than 0.9 as much as possible; for that, C_p was extrapolated linearly and K and ρ were estimated exponentially. Extrapolation was done to be able to compare these materials under hypothetical conditions and determine if these materials are capable of operating in high temperature ranges.

Table A1. Thermophysical properties of different samples used in this study.

| | | | |
|-----------------|--------|---|-----|
| GEO (this work) | C_p | 1000 | |
| | K | 1.2 | |
| | ρ | 2400 | |
| OPC-1 | C_p | $\begin{cases} 0.004521 \times T2 + (-0.6148 \times T) + 802.5 \rightarrow if T \leq 400 \\ 1.05 \times T + 860 \rightarrow if T > 400 \end{cases}$ | |
| | K | $(5.081e + 54) \times exp(-((T - (-1.963e + 05)) / (1.757e + 04))2)$ | |
| | ρ | $71.4 \times exp((-0.004057) \times T) + 2240 \times exp((5.283e - 07) \times T)$ | |
| OPC-2 | C_p | $(0.7 + 8.75 \times 10(-4) \times T) \times 1000$ | [2] |
| | K | $1.467 - 6.667 \times 10(-4) \times T$ | [2] |
| | ρ | 2250 | [2] |

¹ Specific heat capacity (W s/kg °C). ² Thermal conductivity (W/m °C). ³ Density (kg/m³). T is temperature (°C).

Appendix B

This section shows the tabulated properties in Appendix A as graphs; in this part, graphs of thermal diffusivity coefficient and volumetric heat capacity as two important factors in the study of thermal energy storage systems are also prepared. The graphs are density (kg/m^3), specific heat ($\text{J/kg} \text{ } ^\circ\text{C}$), thermal conductivity ($\text{W/m} \text{ } ^\circ\text{C}$), thermal diffusivity (m^2/s) and volumetric heat capacity ($\text{J/m}^3 \text{ } ^\circ\text{C}$) as a function of temperature in the range of 100 to 700 $^\circ\text{C}$.

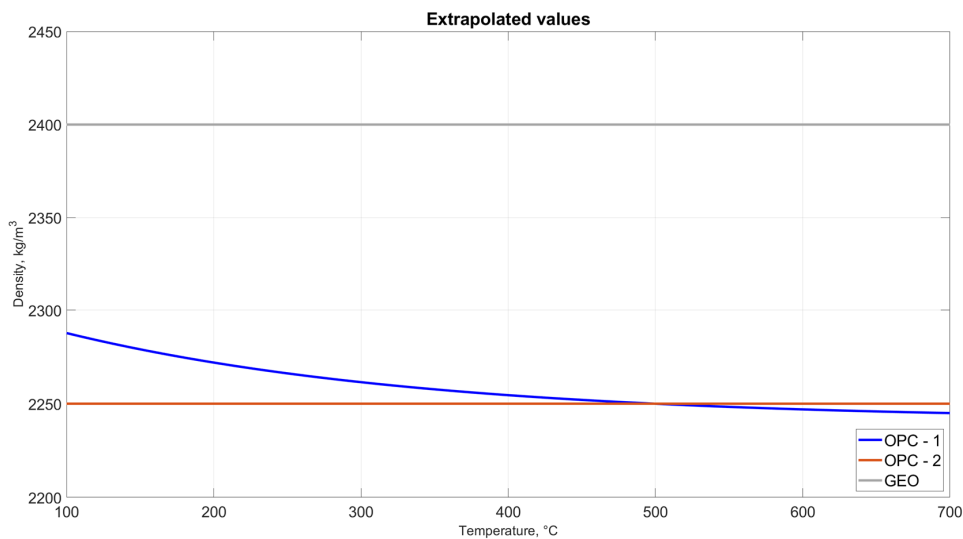


Figure A1. Density (kg/m^3) as a function of temperature.

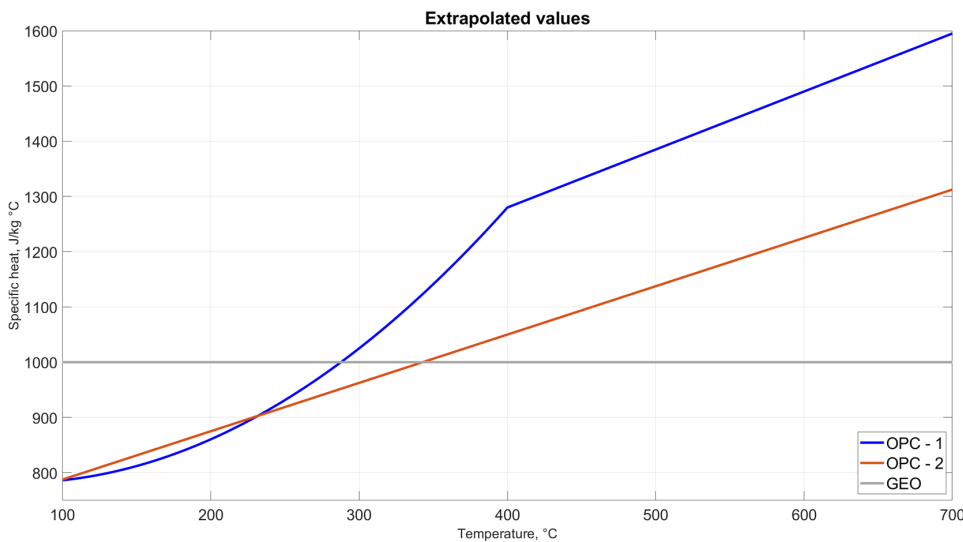


Figure A2. Specific heat ($\text{J/kg} \text{ } ^\circ\text{C}$) as a function of temperature.

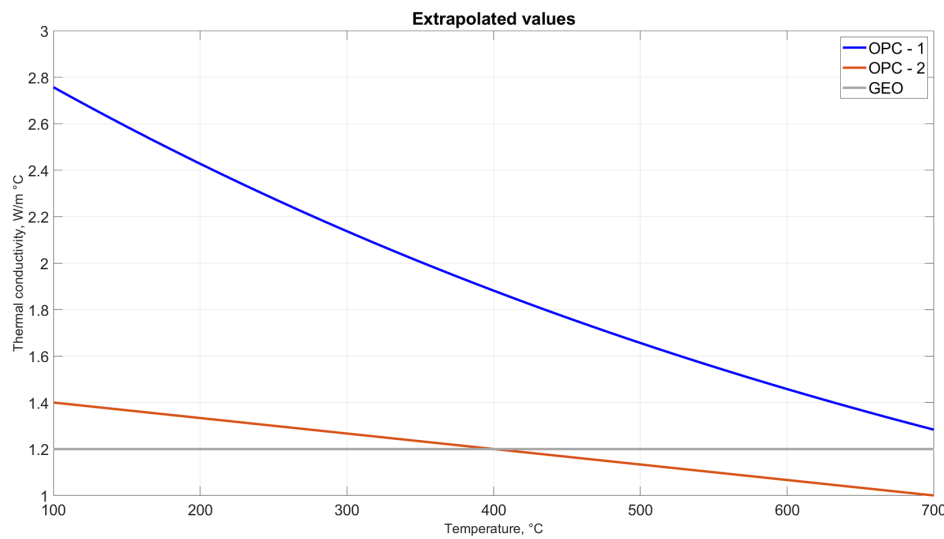


Figure A3. Thermal conductivity ($\text{W}/\text{m} \text{ } ^\circ\text{C}$) as a function of temperature.

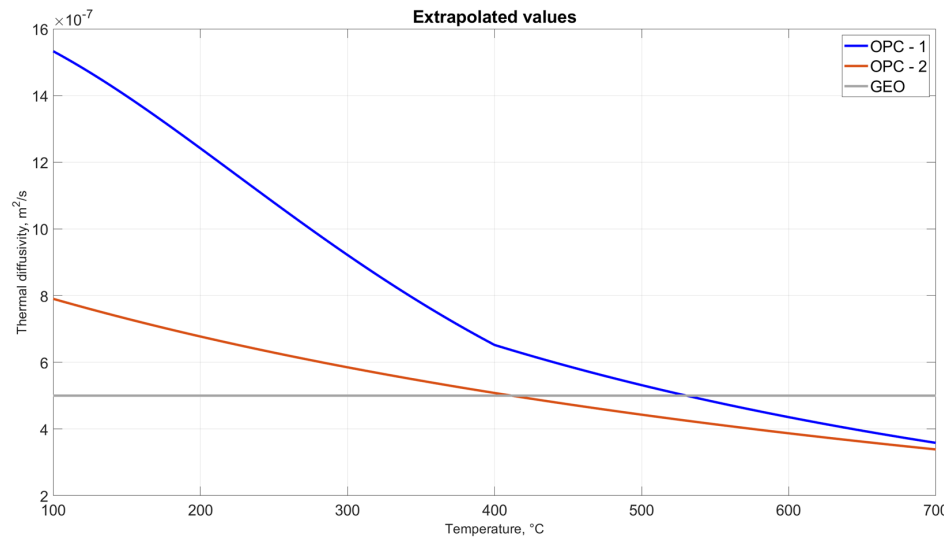


Figure A4. Thermal diffusivity (m^2/s) as a function of temperature.

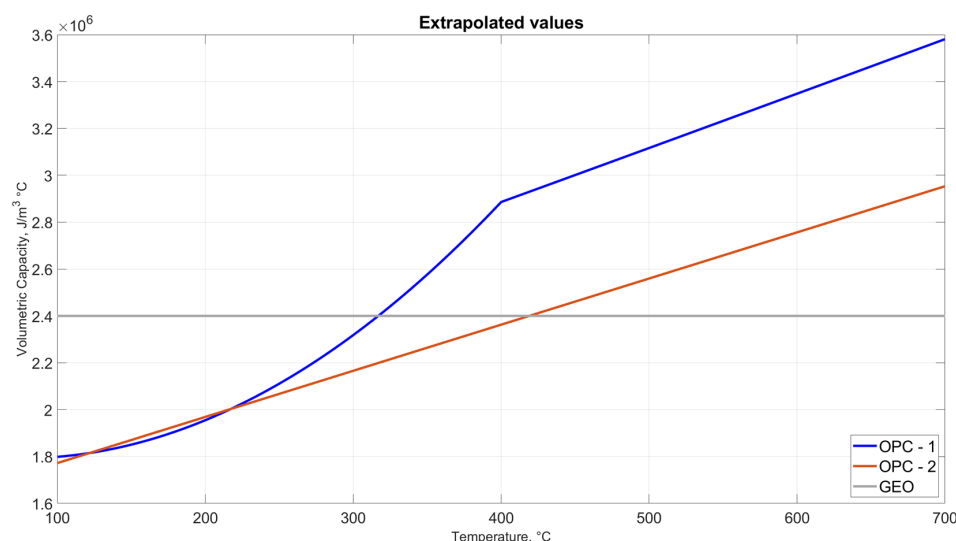


Figure A5. Volumetric heat capacity ($\text{J}/\text{m}^3 \text{ } ^\circ\text{C}$) as a function of temperature.

Appendix C. Grid Independence Test

Triangular quadratic mesh was adopted in the numerical model. In order to test the dependency of numerical results on the mesh element size, a simulation was run by considering that the module is initially at 200 °C and $T_{inlet} = 700$ °C. After 6 h, the average temperature of three different materials was computed. Then $T_{average}$ was compared for different element sizes and runs. It can be observed, in Figure A6 below, that in the range of 40,000–50,000 elements, the difference between $T_{average}$ values of different runs (different element numbers) is less than 0.1% and can be taken for the numerical models as a reliable and accurate result.

$$Difference = \frac{T_{n+1} - T_n}{n}$$

Grid Analysis

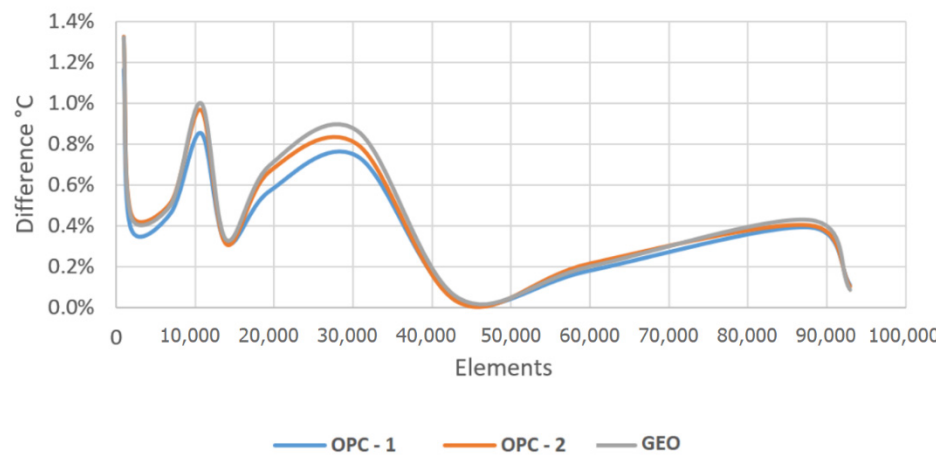


Figure A6. Grid dependency analysis.

Grid Independence Analysis

As shown in Figure A7 below, for the number of elements more than 6000, total elements shape quality stands from 0.9 and tends to reach 1. In conclusion, the meshing should be based on a comprehensive review of CPU usage time, mesh quality and accuracy.

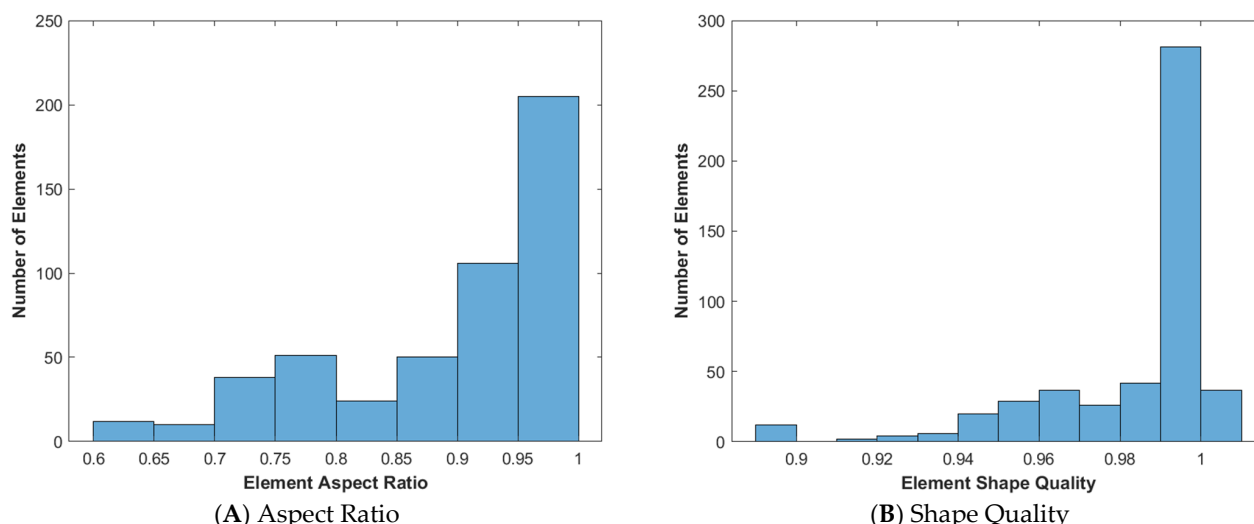


Figure A7. (A) Aspect Ratio (ratio of minimal to maximal dimensions of an element) observed based on geometry and element size growth. (B) Element shape quality for elements = 6924. The quality values are numbers from 0 through 1, where 1 corresponds to the optimal shape of the element.

References

- Laing, D.; Steinmann, W.-D.; Tamme, R.; Richter, C. Solid media thermal storage for parabolic trough power plants. *Sol. Energy* **2006**, *80*, 1283–1289. [[CrossRef](#)]
- Laing, D.; Bahl, C.; Bauer, T.; Fiss, M.; Breidenbach, N.; Hempel, M. High-Temperature Solid-Media Thermal Energy Storage for Solar Thermal Power Plants. *Proc. IEEE* **2012**, *100*, 516–524. [[CrossRef](#)]
- Hoivik, N.; Greiner, C.; Barragan, J.; Iniesta, A.C.; Skeie, G. Long-term performance results of concrete-based modular thermal energy storage system. *Energy Storage* **2019**, *74*, 100735. [[CrossRef](#)]
- Bai, F.; Chao, X. Performance analysis of a two-stage thermal energy storage system using concrete and steam accumulator. *Appl. Therm. Eng.* **2011**, *31*, 2764–2771. [[CrossRef](#)]
- Emerson, J.; Hale, M.; Selvam, P. Concrete as a thermal energy storage medium for thermocline solar energy storage systems. *Sol. Energy* **2013**, *96*, 194–204.
- Skinner, J.E.; Strasser, M.N.; Brown, B.M.; Panneer Selvam, R. Testing of high-performance concrete as a thermal energy storage medium at high temperatures. *Sol. Energy Eng.* **2014**, *136*, 021004. [[CrossRef](#)]
- Laing, D.; Steinmann, W.-D.; Fiß, M.; Tamme, R.; Brand, T.; Bahl, C. Solid Media Thermal Storage Development and Analysis of Modular Storage Operation Concepts for Parabolic Trough Power Plants. *Sol. Energy Eng.* **2008**, *130*, 011006. [[CrossRef](#)]
- Laing, D.; Bahl, C.; Bauer, T.; Lehmann, D.; Steinmann, W.-D. Thermal energy storage for direct steam generation. *Sol. Energy* **2011**, *85*, 627–633. [[CrossRef](#)]
- Salomoni, V.A.; Majorana, C.E.; Giannuzzi, G.M.; Miliozzi, A.; Di Maggio, R. Thermal storage of sensible heat using concrete modules in solar power plants. *Sol. Energy* **2014**, *103*, 303–315. [[CrossRef](#)]
- Ndiaye, K.; Ginestet, S.; Cyr, M. Thermal energy storage based on cementitious materials: A review. *AIMS Energy* **2018**, *6*, 97–120. [[CrossRef](#)]
- Keith, L.; Steinmann, W.-D. *Concentrating Solar Power Technology: Principles, Developments and Applications*; Woodhead Publishing Limited: Sawston, UK, 2012.
- Andiç-Çakır, Ö.; Çopuroğlu, O.; Ramyar, K. Effect of high temperature on mechanical and microstructural properties of cement mortar. In Proceedings of the 11th International Conference on Durability of Building Materials and Components, Istanbul, Turkey, 11–14 May 2008; Istanbul Technical University: Istanbul, Turkey, 2008.
- John, E.E.; Hale, W.M.; Selvam, R.P. Panneer Selvam, R. Effect of high temperatures and heating rates on high strength concrete for use as thermal energy storage. *Energy Sustain.* **2010**, *43956*, 709–713.
- Cuesta, A.A.; Aranda, M.A.G. Belite cements and their activation. *Concr. Res.* **2021**, *140*, 106319. [[CrossRef](#)]
- Guerrero, S.G.; Moragues, A.; Dolado, J.S. Microstructure and mechanical performance of belite cements from high calcium coal fly ash. *Am. Ceram. Soc.* **2005**, *88*, 1845–1853. [[CrossRef](#)]
- Ukrainczyk, N.; Matusinović, T. Thermal properties of hydrating calcium aluminate cement pastes. *Cem. Concr. Res.* **2010**, *40*, 128–136. [[CrossRef](#)]
- Palomo, M.G.; Blanco, M. Alkali-activated fly ashes: A cement for the future. *Cem. Concr. Res.* **1999**, *29*, 1323–1329. [[CrossRef](#)]
- Duxson, P.; Fernández-Jiménez, A.; Provis, J.; Lukey, G.; Palomo, A.; van Deventer, J. Geopolymer technology: The current state of the art. *J. Mater. Sci.* **2007**, *42*, 2917–2933. [[CrossRef](#)]
- Provis, J.L.; Lukey, G.C.; van Deventer, J.S. Do geopolymers actually contain nanocrystalline zeolites? A reexamination of existing results. *Chem. Mater.* **2005**, *17*, 3075–3085. [[CrossRef](#)]
- Puertas, F.; Palacios, M.; Manzano, H.; Dolado, J.; Rico, A.; Rodríguez, J. A model for the C-A-S-H gel formed in alkali-activated slag cements. *J. Eur. Ceram. Soc.* **2011**, *31*, 2043–2056. [[CrossRef](#)]
- Sakulich, R. Reinforced geopolymer composites for enhanced material greenness and durability. *Sustain. Cities Soc.* **2011**, *1*, 195–210. [[CrossRef](#)]
- Ferone, F.C.; Frattini, D.; Roviello, G.; Cioffi, R.; Maggio, R. Finite Element Method Modeling of Sensible Heat Thermal Energy Storage with Innovative Concretes and Comparative Analysis with Literature Benchmarks. *Energies* **2014**, *7*, 5291–5316. [[CrossRef](#)]
- Occhicone, D.F.; Ferone, C.; Cioffi, R. Fibre-Reinforced Geopolymer Concretes for Sensible Heat Thermal Energy Storage: Simulations and Environmental. *Materials* **2021**, *14*, 414. [[CrossRef](#)]
- He, R.; Nan, D.; Wang, Z. Thermal and mechanical properties of geopolymers exposed to high temperature: A literature review. *Adv. Civ. Eng.* **2020**, *2020*, 1–17. [[CrossRef](#)]
- Rivera, W.L.; Weiss Jr., C.; Moser, R.; Williams, B.; Torres-Cancel, K.; Gore, E.; Allison, P. Effect of elevated temperature on alkali-activated geopolymeric binders compared to portland cement-based binders. *Cem. Concr. Res.* **2016**, *90*, 43–51. [[CrossRef](#)]
- Allen, J.; Thomas, J.J.; Jennings, H.M. Composition and density of nanoscale calcium–silicate–hydrate in cement. *Nat. Mater.* **2007**, *6*, 311–316. [[CrossRef](#)] [[PubMed](#)]
- Lolli, F.; Manzano, H.; Provis, J.L.; Bignozzi, M.C.; Masoero, E. Atomistic Simulations of Geopolymer Models: The Impact of Disorder on Structure and Mechanics. *ACS Appl. Mater. Interfaces* **2018**, *10*, 22809–22820. [[CrossRef](#)] [[PubMed](#)]
- The MathWorks. Partial Differential Equation Toolbox. 2020. Available online: <https://www.mathworks.com/help/pde/> (accessed on 1 January 2021).
- Martaúz, P.; Janotka, I.; Strigáć, J.; Bačuvčík, M. Fundamental properties of industrial hybrid cement: Utilization in ready-mixed concretes and shrinkage-reducing applications. *Mater. Construcción* **2016**, *66*, e084. [[CrossRef](#)]

30. Ricklefs, A.M.T.; Falzone, G.; Sant, G.; Pilon, L. Thermal conductivity of cementitious composites containing microencapsulated phase change materials. *Int. J. Heat Mass Transf.* **2017**, *104*, 71–82. [[CrossRef](#)]
31. Streb, F.; Mengel, M.; Schweitzer, D.; Kasztelan, C.; Schoderböck, P.; Ruhl, G.; Lampke, T. Characterization methods for solid thermal interface materials. *IEEE Trans. Compon. Packag. Manuf. Technol.* **2017**, *8*, 1024–1031. [[CrossRef](#)]
32. Tyner, E.; Sutherland, J.P.; Gould, J.W.R. Solar Two: A Molten Salt Power Tower Demonstration. 1995. Available online: <https://www.osti.gov/servlets/purl/100002> (accessed on 21 March 2021).
33. Burgaleta, J.I.; Arias, S.; Ramirez, D. Gemasolar, the first tower thermosolar commercial plant with molten salt storage. *SolarPACES* **2011**, *2011*, 20–23.